Supplementary Information for: Volumetric measurements of wake impulse and kinetic energy for evaluating swimming performance

Derek J. Li[1] and Leah Mendelson[1]

[1] Department of Engineering, Harvey Mudd College, Claremont, CA 91711, USA

S1 Synthetic Trials

S1.1 Impulse Noise Distribution

Uniform noise at each location within the measurement volume produces a regular normal profile of the mean error around 0. Fig. S1 shows an example for an origin at $(0, 0, 0)$ and a resolution of $\kappa = 20$.

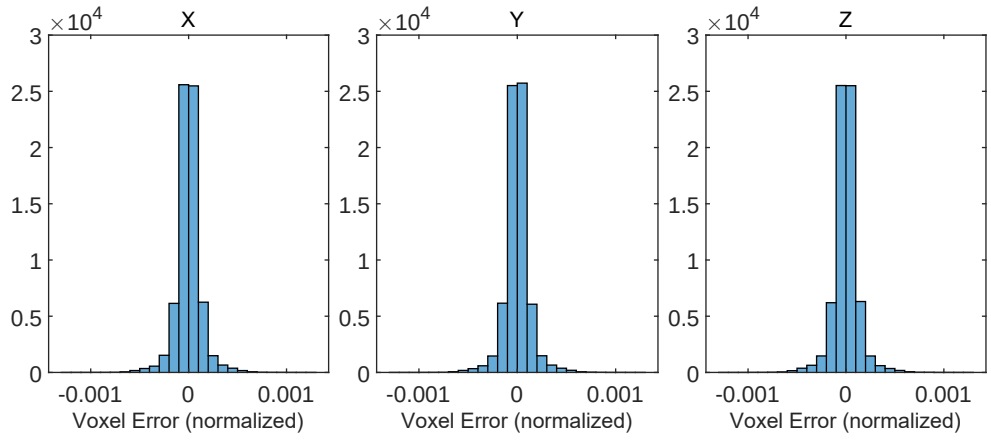

Figure S1: Histograms of the impulse error due to noise for each voxel of a volume with resolution $\kappa = 20$ at noise level $\frac{\delta u}{u_0} = 1.5$. Values are normalized by the total impulse of the Hill's vortex. Errors are normally distributed and have identical profiles across all 3 dimensions.

S1.2 Choice of Noise Model

A normal profile of error for the impulse integrand is also obtained with an alternative noise model (McClure and Yarusevych, 2017) including local and global noise scaling (using two parameters α

and β) and local spatial correlations:

$$\sigma_{i,j,k} = \alpha u_0 \frac{|\nabla \vec{u}|}{\max |\nabla \vec{u}|} + \beta \frac{SF}{\delta t}. \tag{S1}$$

$\sigma_{i,j,k}$ is the standard deviation of a uniform variable corresponding to a component of noise at a grid position, u_0 is the freestream speed and $|\nabla \vec{u}|$ the L_2 norm of the velocity gradient tensor. The three components of noise are modeled with independent variables. In addition to the local scaling of $\sigma_{i,j,k}$, local spatial correlation to represent window overlap is added using a correlation matrix constructed using a triangle function as in McClure and Yarusevych (2017).

Using eqn. S1 and locally correlated noise did not significantly alter impulse errors (fig. S2). We used a uniform window of $w = 32$ voxels and an overlap ratio of $o = 0.75$. Following McClure and Yarusevych (2017), we chose $\alpha = 25\%$ and $\beta = 0.25$px. As before, the origin for impulse calculation is chosen at $(0, 0, 0)$.

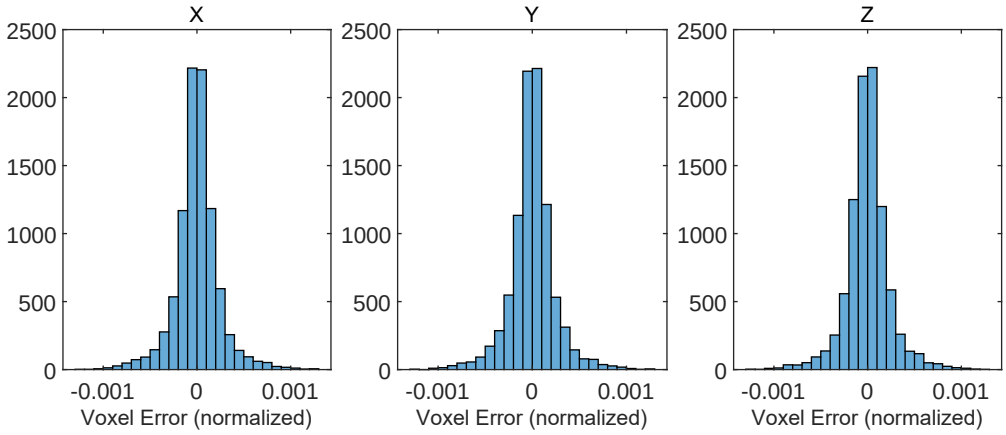

Figure S2: Histograms of the impulse error due to noise for each voxel of a volume with resolution $\kappa = 20$ using a two-parameter noise model with spatial correlation. Values are normalized by the total impulse of the Hill's vortex. Errors are normally distributed and have identical profiles across all 3 dimensions.

S1.3 Impulse Origin

Origin Characterization To characterize the effect of origin selection on impulse error, we constructed a Hill's vortex of resolution $\kappa = 20$ and introduced 150% noise. When no noise is added, a normalized resolution error of 0.007 is shared among all origins. Figure S3a shows the

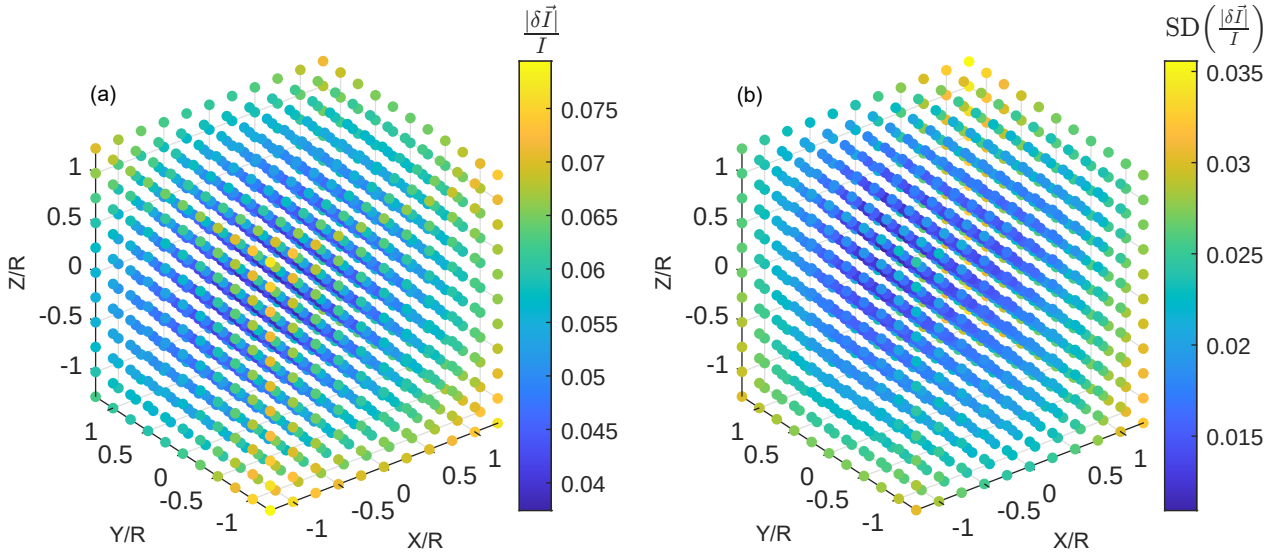

Figure S3: Impulse error magnitude and standard deviation at different origin locations. (a) Mean error of impulse calculation with different choices of origin. Impulse was computed from a Hill's vortex of resolution $\kappa = 20$, under 150% noise, for 20 random instantiations of noise. (b) Standard deviation over these 20 iterations.

mean errors over 20 random iterations of computed impulse using uniformly sampled locations as origins. Impulse errors and their standard deviations between trials (fig. S3b) are lowest at the central origins, while the vertices of the edges incur the highest errors and standard deviations. Since impulse noise propagation is independent of the flow field, this relative profile of error is general under the same noise model.

Objective Origin In the two identities defining the objective origin from DeVoria et al. (2014), impulse appears in the first along with momentum and a surface integral term. We choose to optimize this condition to obtain an origin for calculating impulse:

$$\int_V \rho\vec{u}\, dV - \frac{1}{2}\rho\int_V (\vec{x}-\vec{x}_0)\times\vec{\omega}\, dV + \frac{1}{2}\rho\oint_S (\vec{x}-\vec{x}_0)\times\hat{n}\times\vec{u}\, dS \equiv \vec{\epsilon}, \tag{S2}$$

where $\vec{\epsilon}$ is the residual whose magnitude we minimize. Example objective origin locations, impulse errors, and residuals $|\vec{\epsilon}|$ are shown in figure S4. Most objective origins are in the vortical region distributed around the natural origin, in the vicinity of which we expect a local minimum. In general, the objective origin obtained through optimization reduces error even if not a global minimum of the residual. Comparing the error and residual profiles for the objective origin, we observe a degree

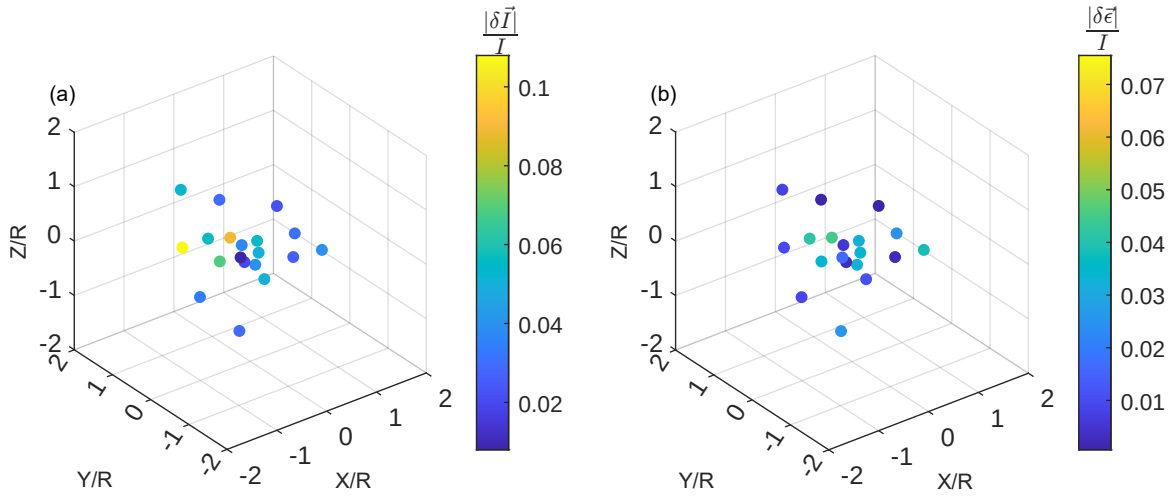

Figure S4: Impulse errors and momentum identity residuals using optimized objective origins. All cases use a Hill's vortex of $\kappa = 20$ exposed to 150% noise. (a) Impulse error magnitude. (b) Residual of momentum identity ($|\vec{\epsilon}|$) normalized by the theoretical impulse. An extreme outlier at position $(-26.93, 11.46, -11.54)$ is omitted from the graph, which has normalized error 0.0617 and residual 0.0624.

of resemblance, though notably there are occasionally objective origins identified far from the region of interest with moderate residual.

In all trials, we initialized our optimization at the centroid. Stochastic optimizers (e.g., the *patternsearch* function in Matlab) performed less well in reducing error than typical optimizers using numerical or analytical gradients, which yielded results of comparable levels of error when no additional constraints are placed on the optimization. Had we optimized both of the identities that DeVoria et al. (2014) used for force calculation, the impulse error becomes higher, especially at higher levels of noise.

S2 Turbulent Vortex Ring

S2.1 Planar Comparison

Planar Impulse Calculation Planar comparisons were performed for the spatiotemporally smoothed data. Impulses for the planar comparison were calculated at each timestep from the center XY plane of the flow field using an axisymmetric vortex ring model (eqn. S3).

$$\vec{I} = \rho \Gamma \pi R^2 \tag{S3}$$

A threshold of 25% of the maximum vorticity magnitude was applied to locate the vortex cores. Circulation in each vortex core was calculated as the area integral of all same-signed vorticity above the threshold. A correction factor ($\Gamma_{thr} = (1 - 0.25)\Gamma$) was applied to the circulation data to account for the choice of threshold (Spedding et al., 2003). Circulations were averaged between the positive and negative vortex cores. Vortex ring diameters were estimated as the distance between the centroids of the positive and negative vortex cores.

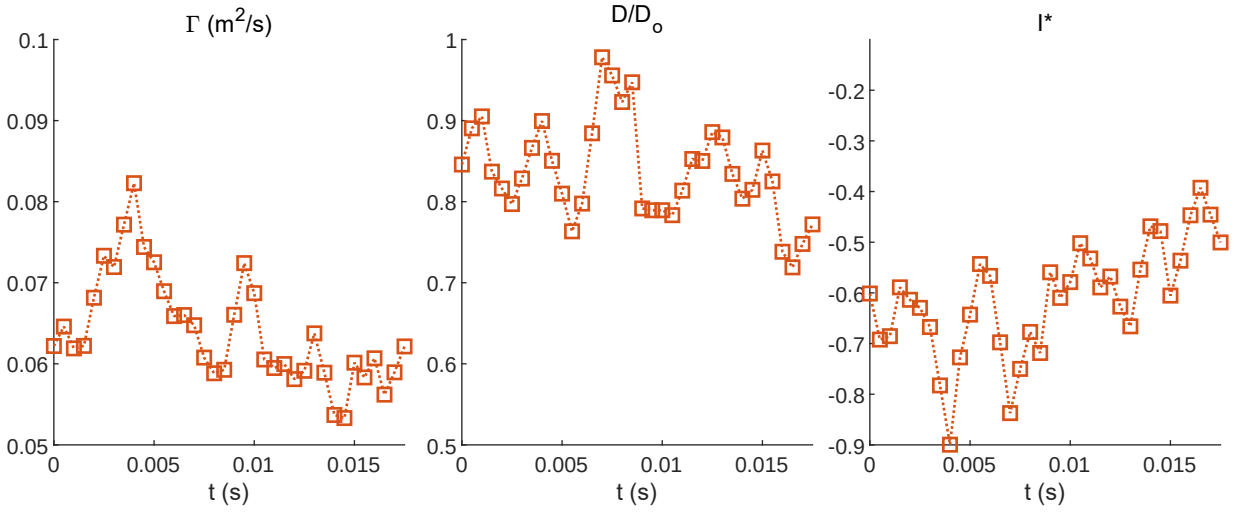

Figure S5: Circulations, diameters (normalized by the nozzle diameter), and impulses (normalized by the slug impulse) calculated over time for the center XY plane of the spatiotemporally smoothed turbulent vortex ring data.

S2.2 Impulse Domain Selection

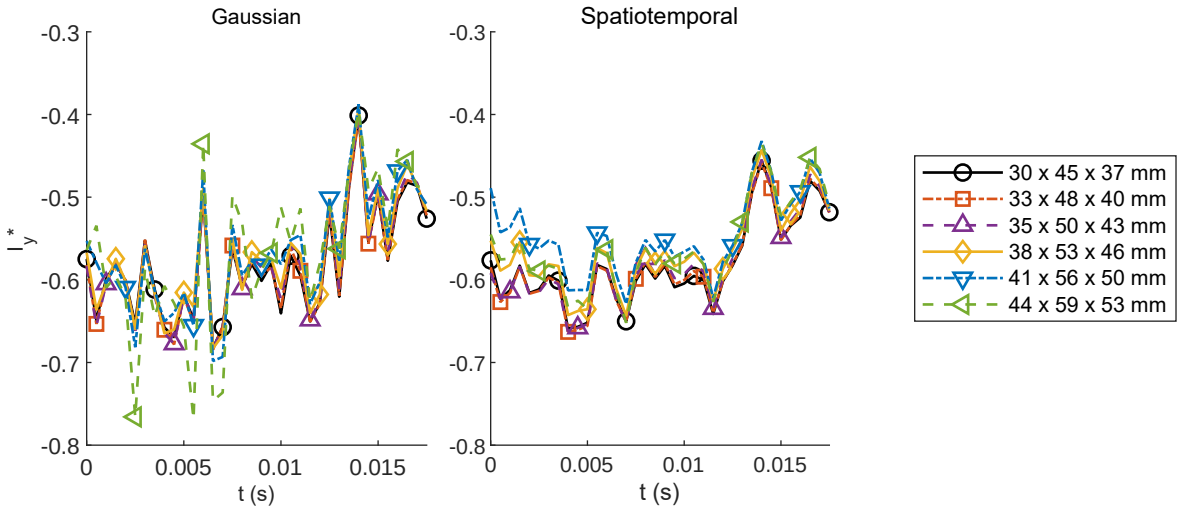

Figure S6: Normalized axial impulses calculated for each of the six integration domains considered for the turbulent vortex ring case.

S2.3 Kinetic Energy Smoothing

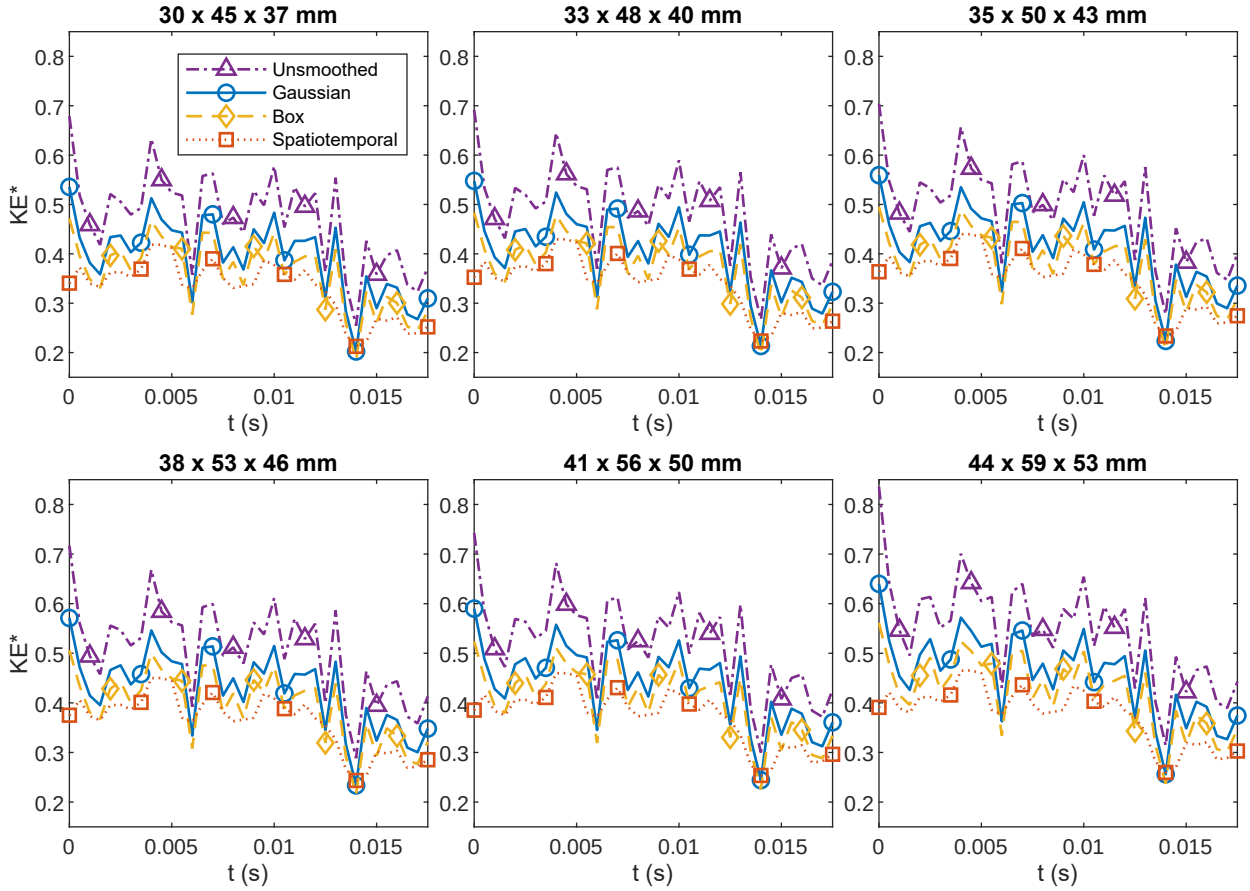

Figure S7: Normalized kinetic energies over each time for each field of view and smoothing option. Smoothing had a significant effect on the energy calculated.

S3 Turning Fish

S3.1 Planar Comparison

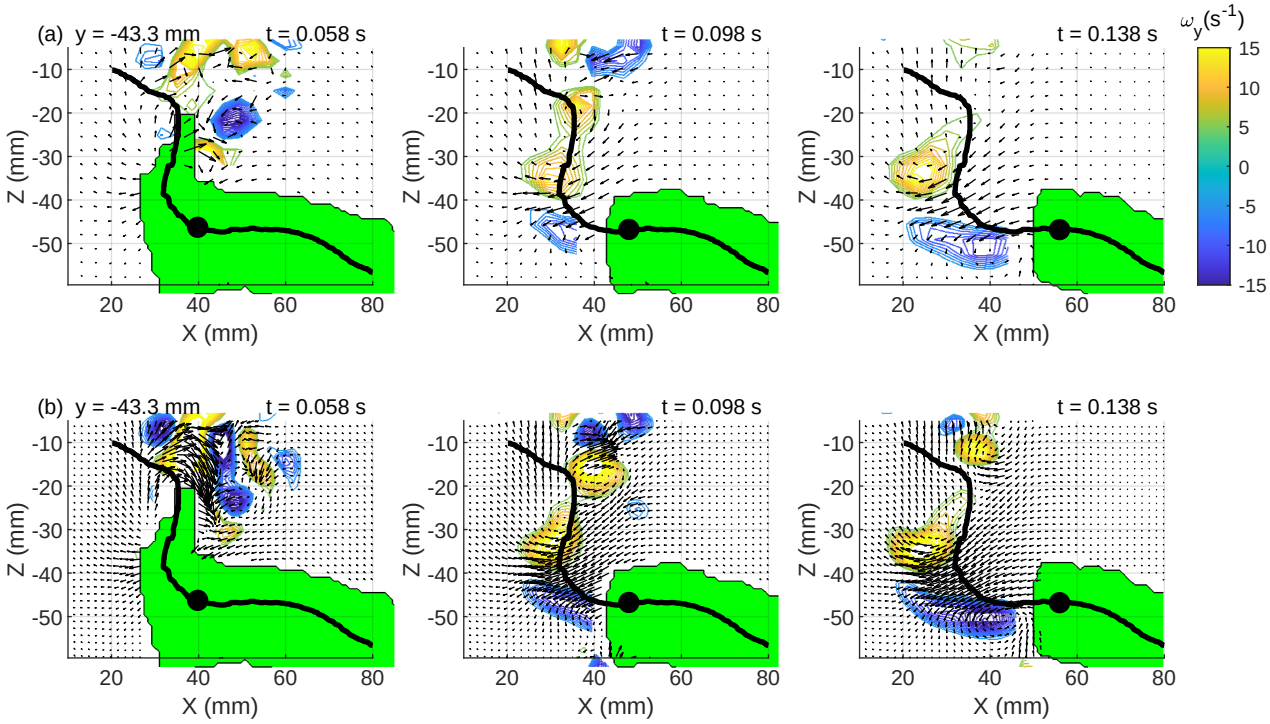

Figure S8: Planar section through the wake in the plane of the caudal peduncle (y = -43.3 mm) with both (a) 50% and (b) 75% window overlap. Contours show the y vorticity component and the green surface is a projection of the fish body visual hull. The solid black line shows the caudal peduncle trajectory, and the circular marker shows peduncle location in each frame.

Planar Impulse Calculation Impulses for the planar comparison were calculated for the larger propulsive vortex at t = 0.138 s using the same procedure as the turbulent vortex ring test case (Section S2.1).

S3.2 Impulse and Energy Fluxes

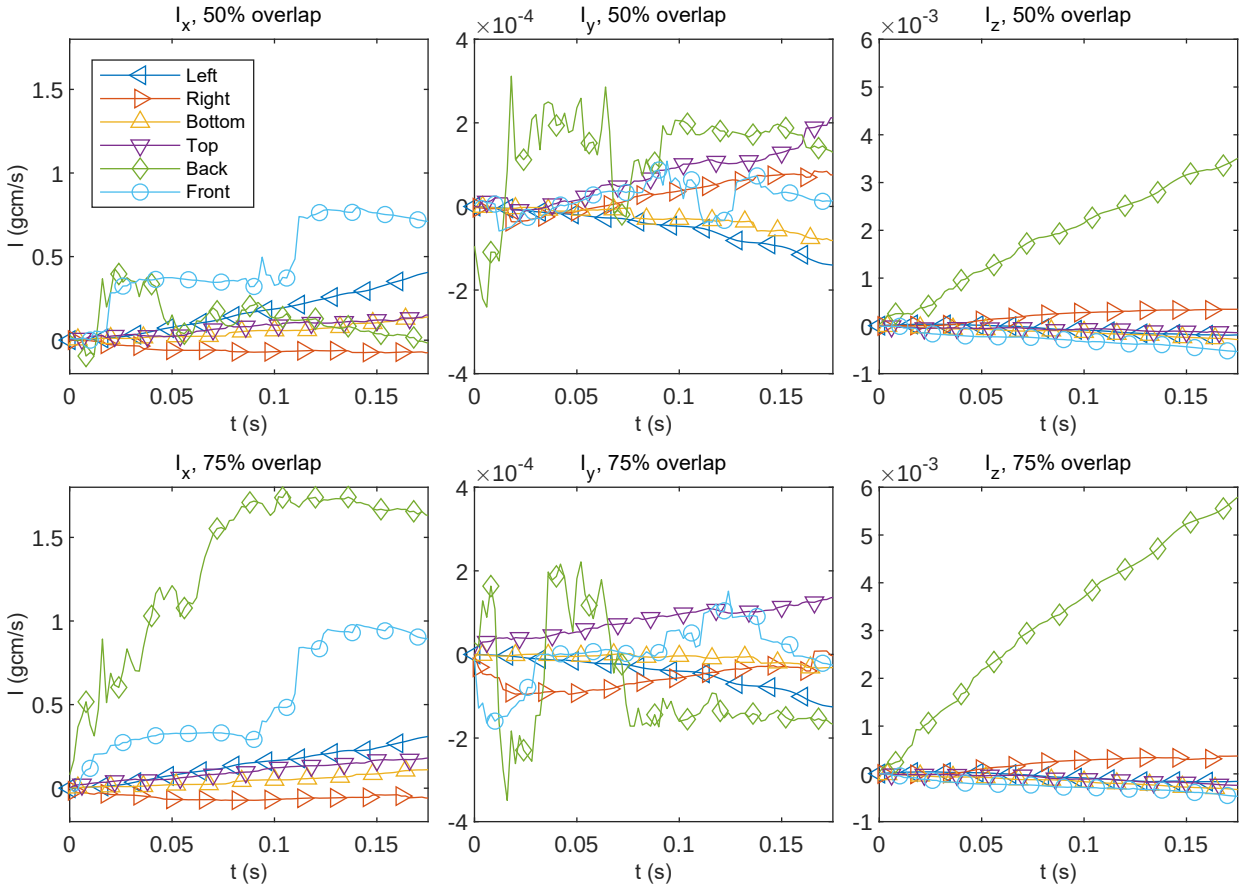

Figure S9: Cumulative impulse fluxes across each surface of the volume for each window overlap. Positive fluxes denote impulse leaving the measurement volume. Losses were small compared to the total impulse in the measurement volume.

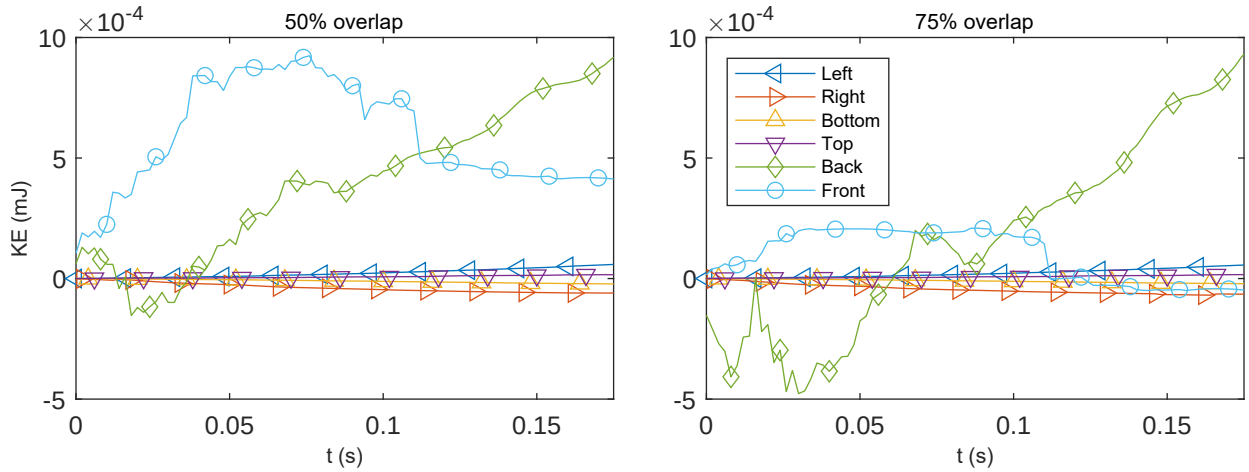

Figure S10: Cumulative energy fluxes across each surface of the volume for each window overlap. Positive fluxes denote kinetic energy leaving the measurement volume. Losses were small relative to the total impulse in the measurement volume and the estimated dissipation.

References

DeVoria A, Carr Z, Ringuette M (2014) On calculating forces from the flow field with application to experimental volume data. J Fluid Mech 749:297–319

McClure J, Yarusevych S (2017) Instantaneous PIV/PTV-based pressure gradient estimation: a framework for error analysis and correction. Exp Fluids 58(8):1–18

Spedding GR, Rosén M, Hedenström A (2003) A family of vortex wakes generated by a thrush nightingale in free flight in a wind tunnel over its entire natural range of flight speeds. J Exp Biol 206(14):2313–2344